Turbine Design Report

James Madison University

Team Member	Sub-Team Affiliation	Individual Role	Contact Information
Jake Abruzzi	Mechanical/Blades	Blade/Generator Design	abruzzjp@dukes.jmu.edu
Roman Cook	Controls/Electronics	Electronics/Controls Programming	cookra@dukes.jmu.edu
Andrew Payne	Controls/Electronics	Electronics/Controls Programming	payne2aj@dukes.jmu.edu
Oumaima Atraoui	Mechanical	Generator Design	atraouox@jmu.edu
Ethan Anderson	Mechanical	Generator Design	ander3ec@dukes.jmu.edu
Jack McGeoghegan	Controls/Blades	Electronics/Controls Programming	mcgeogje@dukes.jmu.edu
Joey Carrico	Mechanical	Yaw	carricjm@dukes.jmu.edu

JMU Principal Investigators: Dr. Stephen K. Holland, Ph.D., Dr. C.K. Lee, Ph.D., Dr. Jonathan Miles, Ph.D.

Table of Contents

Executive Summary

The James Madison University (JMU) 2020 Collegiate Wind Competition (CWC) wind turbine emphasizes four primary design objectives: power production, control, safety, and ease-of-use. Building upon prior competition team experiences, the JMU CWC prototype design team focused on designing the prototype turbine to enhance these four elements, relative to prior designs.

To provide flexibility for power production system design, the team continued use of a custom built, direct drive axial flux permanent magnet generator. The ease of fabrication and customization options afforded by this design allowed the team to consider multiple generator design configurations that could be matched with rotor performance characteristics to maximize the power production capabilities of the turbine. This year, the team focused significant efforts on identifying rotor and generator design pairings, accounting for the torque and rotational speed characteristics, that could optimize the system's power production capabilities. By iterating blade and generator design parameters, including airfoil selections, design tip speed ratios, generator air gap spacing, and coil winding parameters, the team was able to design a synergistic wind power system to maximize power production with a fixed pitch blade system throughout the expected wind speed range.

The cut-out task presented an opportunity to explore additional areas for control system improvement. To achieve accurate control of the turbine and identification of the cut-out conditions, the team sought methods for direct measurement of the wind speed and drive train conditions. Prior teams estimated wind speed conditions based on rotational speed, electronic load settings, and electrical outputs. Following the theme of designing more accurate controls, a method of direct measurement of wind speed and a more accurate RPM measurement device were implemented in the 2020 design. To achieve wind speed measurements, a hollow drive shaft was designed to accommodate a pitot tube for wind speed measurement at the front of the rotor. A new optical disk encoder, replacing an error prone reflective sensor, was also incorporated into the design to increase resolution and accuracy of rotational speed measurements. These improved measurements increase decision making capabilities of the control subsystems.

This improved ability of the turbine's sensors also increased the overall safety of the design. Obtaining accurate values for wind speed and power generation provides more information for the braking subsystems. Through the use of two braking systems, a smart disc brake and an emergency clamp brake, the turbine can be slowed to maintain a safe RPM and parked when power is cut or when disconnected from the PCC.

In order to increase the ease of installation, electrical connection, and use of the turbine during the competition, a compartment was added to the nacelle to house all of the control electronics, eliminating the need for control electronics to be placed outside of the turbine. This design decision, and the use of custom designed printed circuit boards, allowed for all power conditioning, sensing, and control actions to occur within the nacelle, subsequently reducing the number of signal and power cables that would need to be routed through the turbine tower. This also reduced the number of potential electrical connection failure points and minimized potential for analog measurement and control signal degradation through lengthy cables and connectors, enhancing the quality of control and reliability of the turbine. Similarly, safety is enhanced by minimizing the number and type of external connections that must be made to ensure proper and safe operation of the turbine.

The JMU 2020 CWC team has appreciated all of the learning opportunities afforded by this challenge. Despite being unable to complete the construction and testing of the prototype, the team is confident in the design decisions made to enhance the power production capabilities, control, safety, and ease-of-use of this prototype, as described in detail in this report.

1 Design Considerations

1.1 Prioritization of Competition Tasks

The design of the JMU CWC team's small-scale prototype wind turbine is outlined in this report. The prototype turbine was designed to satisfy the competition constraints while maximizing performance in the Power Curve Performance, Control of Rated Power, Safety, and Durability tasks.

To ensure completion and competitive advantage in the prioritized tasks, the team built upon prior competition experiences to enhance the prototype turbine performance. Five unique enhancements from prior designs were incorporated, in addition to other improvements. First, it was recognized that the JMU 2019 CWC team's blade and generator design could benefit from an explicit matching of torque and rotational speed characteristics to optimize operation points. Extensive iterative analysis was performed to ensure that the expected rotor blade characteristics were matched with the home-built generator design to provide optimal power production performance and a relatively low cut-in wind speed. Second, to ensure proper control and safety capabilities, the team sought to develop a method to directly measure the incoming wind speed, instead of inferring it based on rotational speed and generator output measurements. The inclusion of a pitot-tube mounted through a hollow drive shaft allowed for wind speed measurements as the primary control input. Third, a MOSFET based ideal-diode three-phase rectifier was incorporated into the power-conditioning electronics to reduce power losses associated with diode rectification at high wind speed conditions. Fourth, an emergency braking system, used in conjunction with a variable speed disc brake system, was added to maintain a parked condition at high wind speeds. Finally, the undercarriage of the nacelle was modified to accommodate all of the custom printed circuit boards required for power management and control, thus eliminating the need for excessive cabling through the tower to an external control panel.

To identify and map turbine subsystems to competition tasks, the chart shown in Table 1 was developed by the team. This helped guide the design and evaluation of the subsystems. For example, by using this chart the team chose to focus on performance in the cut-in wind speed and power curve performance tasks when evaluating blade and generator design alternatives.

Table 1: *Tasks and Subsystems Table.*

Task	Points	Subsystems					
Cut-in wind speed	25	Blades	Generator				
Power curve performance	50	Blades	Generator	Load side electronics			
Control of rated power and rotor speed	50	Turbine side electronics	Load side electronics	Variable speed brake	RPM sensor	Wind speed sensor	
Safety	50	Variable speed brake	Emergency brake	Wind speed sensor	Turbine side electronics	Load side electronics	
Durability	50	Turbine side electronics	Load side electronics	Variable speed brake	RPM sensor	Wind speed sensor	Yaw system
Cut-out and parked high wind	25	Emergency brake	Wind speed sensor	Variable speed brake			

1.2 Trade-off Analysis

Several trade-offs were considered in the design of the prototype turbine. A primary consideration trade-off decision was the selection of high rotational speed, low torque design, vs. a low rotational speed, high torque design. With a high torque design, the turbine will be able to cut-in at a lower wind speed, however since it spins at a lower RPM, it will not be able to generate as much power in the power curve task. A generator with a high RPM will cut in at a higher wind speed since it will not generate as much torque, however it has potential to generate more power. Experience with prior in-house fabricated axial flux permanent magnet (AFPMG) generators suggested that a higher torque

design with a lower operational speed would provide sufficient cut-in task performance, ensure safety, and reduce the potential for mechanical failures. Pairing high torque blades with a generator that has a high flux density will allow the team to perform well in the power curve task as well. To begin the process of blade and generator design, a tip speed ratio design between 2-3 was selected as a starting point.

2 Design

2.1 Blade and Electrical Power Generation

2.1.1 Design Approach

The team took an iterative, generator first approach when designing blades. That is, various blade designs were compared to a few different direct-drive generator configurations to estimate power production capabilities and suitability of the blades to drive the generator. This approach was taken due to the ability to design, construct, and iterate blades at a much faster rate than the generator. After modeling the torque characteristics of four AFPMGs, it was determined that the blades would need to operate at a TSR between 2 and 3, consistent with experiences from prior teams. An approximate Reynolds number of 75,000 was used to model airfoil and blade performance. When performing calculations, values for the air density, ρ , and viscosity, μ, were based on the lower density air expected at the competition site in Colorado.

Preliminary research on commonly used airfoils in different types of turbines was then done to identify potentially suitable airfoils. The team also used the Airfoil Tools database [11] to search for candidate airfoils with a high lift-to-drag ratio at low Reynolds numbers. Once the team gathered potential airfoils designs, they were input into QBlade [12] for further analysis and blade design. Each potential airfoil was used as the basis for a blade design, using both Schmitz and Betz optimization methods at a variety of TSRs between 2 and 3. Every blade was designed with a hub radius of 4 cm and a blade length of 18 cm to adhere to competition guidelines. The team did consider making a rotor with more than 3 blades, however after running simulations within QBlade it was determined that the added blades did not significantly increase performance, and would just end up adding an extra potential failure point. In essence, designing all of these blades gave the team a large bank of potential blade designs that could then be selected to match with the generator characteristics. In total, over 75 unique blade designs were generated and analyzed as potential designs.

The team planned to test some of these blade designs using a Magtrol TS 106 torque sensor in a wind tunnel to confirm the QBlade predictions. Unfortunately, testing could not be conducted when access to our laboratory space was lost.

2.1.2 Rotor Blade and Generator Matching

The team conducted extensive analysis in order to pair the generator and blades to optimize power production performance. Four generator configurations were constructed and modeled analytically, changing the magnet wire gauge and number of wire turns per coil in each iteration. Neodymium magnets with a residual flux density of 14,800 gauss were used in all generator iterations. The team then used the bank of modeled blades to identify the optimal pairing of rotor designs with each generator. Torque vs. rotational speed curves of the blade candidates were overlaid with the same characteristic curves of the generator at a fixed operational voltage.

The more vertical lines show the torque required to spin the generator at various rotational speeds. Each line represents a different constant-voltage operation characteristic for the generator, where the voltage is maintained constant by varying the generator load resistance. The mountain-like curves show the predicted torque generated by the blades as a function of rotational speed. Each curve represents the torque vs. rotational speed characteristics of the rotor at different constant wind speeds.

The expected steady state operating point for the rotor at a given wind speed and generator voltage can be found by determining the intersection points between the constant-voltage generator curve and the rotor performance curve. By identifying the operational points at a given wind speed, an optimal rotational speed can be identified to maximize power production. This maximum power production operation point analysis was performed for each rotor blade and generator design. A projected score, based on the CWC scoring rubric for the power curve performance task, was calculated based on these analyses.

2.1.3 Resulting Matched Designs

After analyzing the best blade pairings for each generator iteration, the design that would produce the highest score in the Cut-in wind speed and Power Curve Performance tasks was selected. For this design, the team identified the Wortmann FX 60-126 airfoil based blades, optimized using the Schmitz optimization at a design tip speed ratio of 2. The blades have a length of 18 cm, and a hub a radius of 4 cm with three blades comprising the rotor. The parameters for the selected generator can be found in section 2.1.5. The resulting Torque vs. RPM curves of the selected design blade/generator design can be seen in Figure 2.

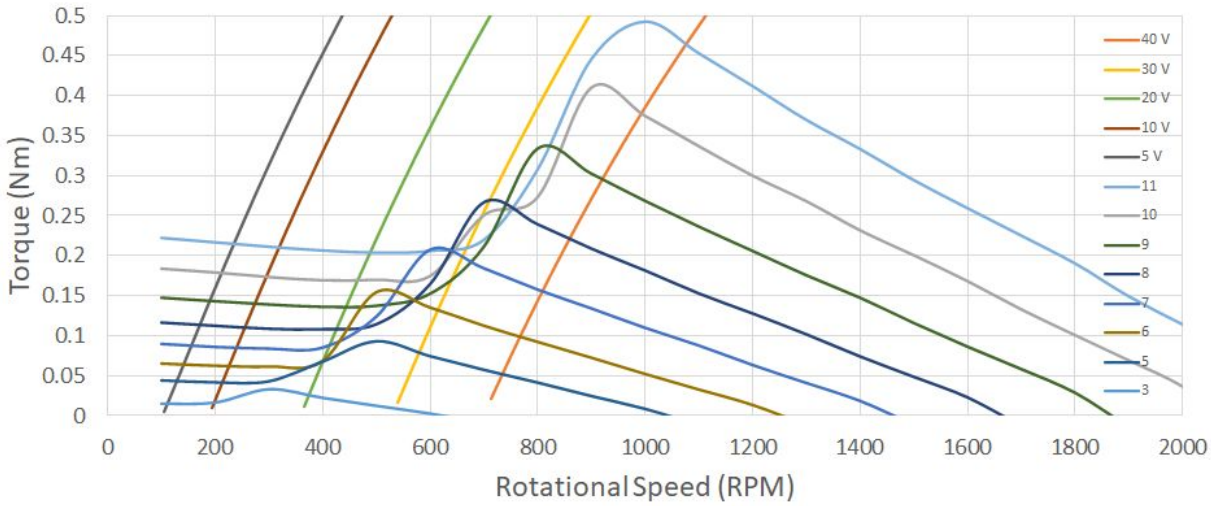

Figure 2: *Torque vs. RPM curves of the selected design*

Using the described generator and rotor matching analysis, the projected power production at each wind speed from 5 to 11 m/s was calculated, resulting in a projected score of 48.55 points in the power curve performance task seen in Table 2.

Table 2: *Projected Power Curve Performance Task Scoring*

Wind Speed (m/s)	Projected Power (W)	Factor	Score
5	4	0.7	2.8
6	7.5	0.8	6
7	10.4	0.8	8.32
8	15.2	0.7	10.64
9	20.7	0.4	8.28
10	29.6	0.3	8.88
11	36.3	0.1	3.63
Total			**48.55**

It should be noted that these calculations are based solely on the power production capabilities of the selected blades and generator pairing and do not take into account losses in the electrical components, including the buck converter and actuators. Thus, it is expected that the scoring in the competition will be lower than these calculations. A team estimated approximately 1W of power consumption from associated control and power conditioning electronics; unfortunately, this assumption has not been tested, as full operation and control tests were slated to occur in April. Based on the simulation analysis, cut-in is expected at wind speeds between 3 m/s and 4 m/s, resulting in a score between 10 and 20 points for the Cut-in Wind Speed task. In preliminary testing the team observed shaft rotation at wind speeds between approximately 2 and 2.5 m/s, however this test was run using a box fan and no load. A projected power curve for the final design is presented in Figure 3.

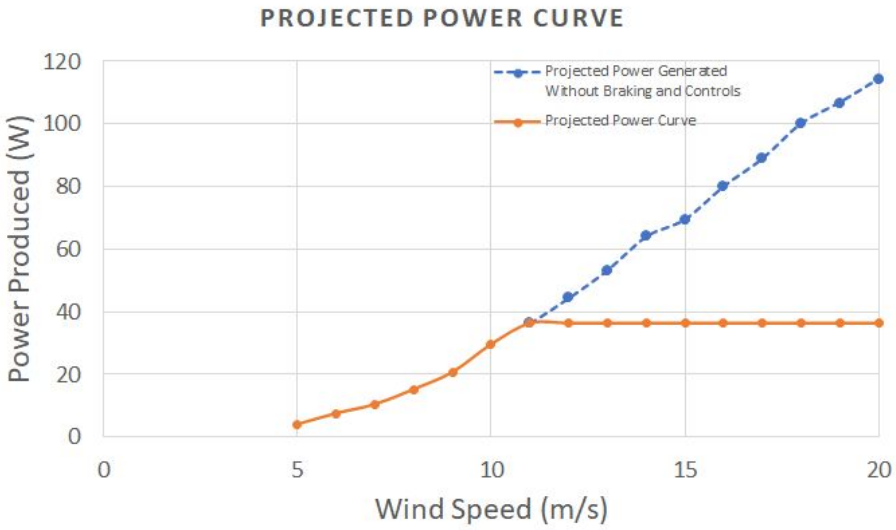

Figure 3: *Projected Power Curve for Selected Design*

The orange line in Figure 3 shows the projected power curve of the turbine. For wind speeds ranging from 5 m/s to 11 m/s the turbine will maximize power production. From 11 m/s to 20 m/s the turbine will maintain a constant power output using the turbine's electromechanical braking and controls scheme, described below. The dotted blue line shows the power that the turbine has potential

to produce from 12 m/s to 20 m/s without any braking or controls. This surplus power shown by the blue dotted line will be used to power the turbine's electromechanical control components and/or dissipated through a power resistor.

2.1.4 Blade Construction

The team examined three design alternatives for blade construction. The first option considered was 3D printing the hub and blades using Onyx, a printable nylon material mixed with carbon fiber, which makes it extremely strong and lightweight [14]. This material was used for blade construction in the previous competitions. Thrust data gathered in QBlade was converted to a point load at the end of the blade so that initial testing could be done by hanging a load from the end of the blade. The test blade was able to stand up to the highest thrust loads expected with negligible bending. The Onyx blades were mounted to the hub using steel screws and locknuts. The second option considered was constructing the blades of fiberglass. This would provide a blade stronger and lighter than the Onyx option. However, due to in-house capabilities and environmental regulations, the carbon fiber blade construction would need to be outsourced. This would leave the team unable to iterate multiple blade concepts. Since Onyx was successful in previous competitions and in preliminary testing, this option was not pursued. The final option considered was creating a one piece mold for the whole rotor using a vacuum sealer, and then filling it with epoxy. This option would produce the strongest rotor since it would only be one piece, eliminating the connection between the hub and blades. While a solid epoxy rotor would be stronger than the Onyx rotor, it would be significantly heavier. After the Onyx rotor was able to function successfully at speeds of up to 2500 RPM in the rotor strength test the team decided to continue with Onyx design and focus efforts on other aspects of the design. The team expects a maximum normal operational rotor speed of approximately 1100 RPM; therefore, based on the results of this test the blades will have a safety factor greater than 2.

2.1.5 Generator Construction

An axial flux permanent magnet generator (AFPMG) was selected due to its ease of construction and its low starting torque characteristics with minimal cogging. The ease of fabrication allowed for multiple designs to be considered for pairing with different rotor designs to optimize power production potential.

The generator consists of two main subsystems, the stator and the rotor. The stator consists of 9 coils that are oriented into a disk and then molded together with an epoxy resin. The stator disk is sandwiched in between two iron rotor disks in order to increase the magnetic flux passing through the coils. Each disk holds 12 Neodymium magnets that are oriented to pass each coil at exactly 30 degrees. A mold was 3D printed and epoxied onto each plate in order to keep each magnet in place and to prevent them from shifting during rotation.

Increasing the number of wire turns present in a single coil increases the voltage output of the generator, but also increases resistance losses in the generator. Additionally, increasing the turns of wire also increases the thickness of the stator, necessitating increased air-gap spacing between the permanent magnets and rotor plates. Increasing the air gap between the rotor plates, in turns, decreases the magnetic flux, thereby decreasing the power production potential. Similarly, the number of coil turns and wire gauge used impacts the torque required to rotate the generator under loaded conditions.

As described previously, a mathematical model was created to identify how these parameters impacted the torque vs. rotational speed characteristics of the generator at a constant voltage output. Four candidate designs, shown in Table 3, were identified and used in the simulations to identify an optimal rotor and generator design paring. The selected and fabricated stator design has nine coils, each

comprising 250 turns of 26 gage wire. Three sets of three coils, connected in series, form the three phases of the generator. These series connected coil phases are connected in a Wye or star configuration.

Table 3: *Stator Design Parameters*

	# of Phases	# of Coils	# of Turns	Coil Shape	Configuration	Wire Gauge
Alternate Stator	3	9	300	Tear Drop	Wye	28
Selected Stator	3	9	250	Tear Drop	Wye	26
Alternate Stator	3	9	225	Tear Drop	Wye	26
Alternate Stator	3	9	225	Tear Drop	Wye	28

2.2 Mechanical Design

2.2.1 Nacelle/Housing

Prior competition teams used an optical reflector to measure rotor rotational speed; however, this reflection method was prone to errors and did not have sufficient resolution for low speed measurement. To enhance the accuracy of rotational speed measurement, a new optical encoder was included in this design. Additionally, the team incorporated a pitot tube into the drive shaft design to improve control based off of direct wind speed measurements. Finally, an emergency braking system to address the parked wind speed durability challenge was added.

To accommodate these additions and modifications, a nacelle redesign was performed. The nacelle was designed to be constructed out of the same lightweight 6061 aluminum. The nacelle was lengthened to accommodate these additional additions. Figures 4 and 5 present a final assembly model of the nacelle, including electronic components, with callouts for components of interest.

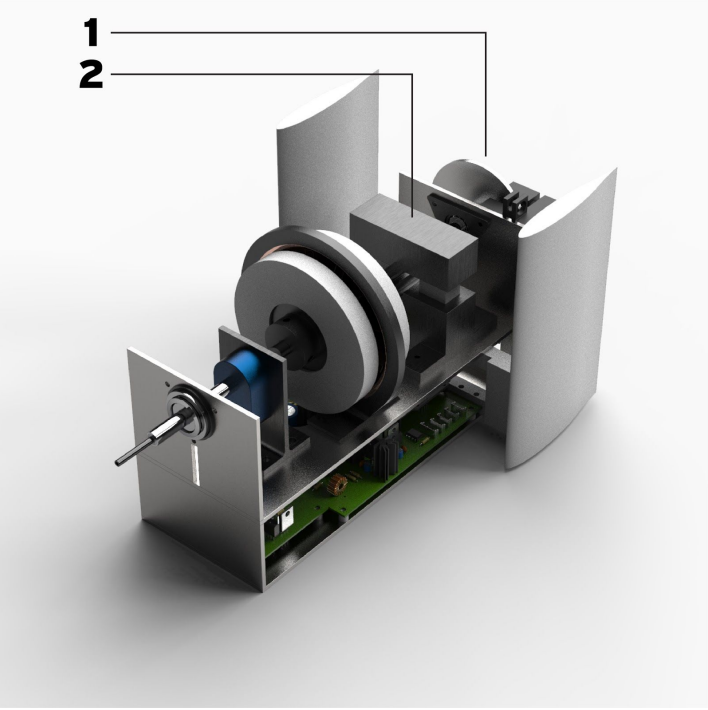

Figure 4: *Labeled Nacelle Model*

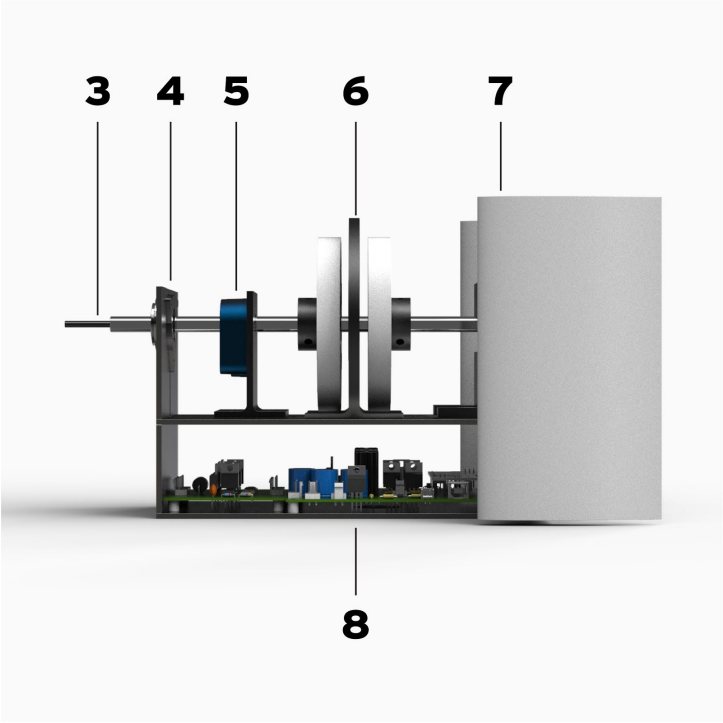

Figure 5: *Labeled Nacelle Model*

In Figure 4, the emergency brake (1) is used during the Emergency Shutdown and Parked High Wind Speed tasks. When the emergency brake is triggered, two linear actuators will cause the mechanism to clamp the shaft. The selected PQ12 linear actuators have a 100:1 gear ratio and will retain the clamped force even when power is lost as a result of slowing the rotor and generator. Also visible in the back of Figure 7 is a disk brake system. This disk brake uses a rotary servo motor to clamp a brake caliper on the disk (2) with variable pressure. Used in the previous competitions, this disk brake will be used to provide variable braking during the Control of Rated Power tasks.

Figure 5 shows the newly included pitot tube (3), which protrudes from the front of the nacelle and passes through the rotor hub. The ⅛ inch diameter pitot tube passes through the rotary drive shaft, mounted in micro ball bearings. The pitot tube is used to measure the stagnation pressure of the incoming air flow, which is used along with a static reading taken from inside the nacelle to calculate the incoming wind speed. This novel aspect of our design will allow for the turbine controls to monitor and adjust performance based on direct measurement of the incoming wind speed. A torsional stress calculation on the hollow shaft was performed to confirm a safety factor of over 10 at the highest expected shaft load, mitigating concerns that the aluminum shaft could deform.

A thrust bearing (4) is used at the front of the nacelle to prevent the shaft from moving forward or backward during operation. The optical encoder with a custom mount (5) was added to the turbine in order to more accurately determine the rotational speed of the shaft during operation. The previously described AFPMG (6) can be seen after the optical encoder and is made up of a stator sandwiched between two rotors. The new yaw fins (7) are part of our passive yaw system used to position the turbine directly facing the incoming wind. Since the size of nacelle was increased, the team positioned yaw fins on either side of the turbine to remain within the competition size guidelines. Finally, an electronics compartment (8) was added to the nacelle in order to minimize wiring coming out of the turbine enclosure. The AC/DC rectification circuit, power conditioning circuit, and the turbine-side Arduino microcontroller will be placed in this compartment.

2.2.2 Yaw Design

The turbine utilizes a passive yaw system. The passive yaw system consists of two ball bearings with an inner diameter of 1.5”and two linear ball bearings press fit around the aluminum shaft serving as the tower. The custom made 3D printed pieces shown in Figure 6 serve as a housing for the ball bearings and a connection point to the nacelle. The yaw system is connected to the nacelle via four bolts. The ball bearings in the design allow the nacelle to move freely atop the tower. The team performed calculations [18] to determine the force generated by the symmetrical airfoil yaw fins at different wind speeds. Initial calculations for the size angle of the yaw fins were performed, however this testing could not be completed due to the restrictions placed upon us.

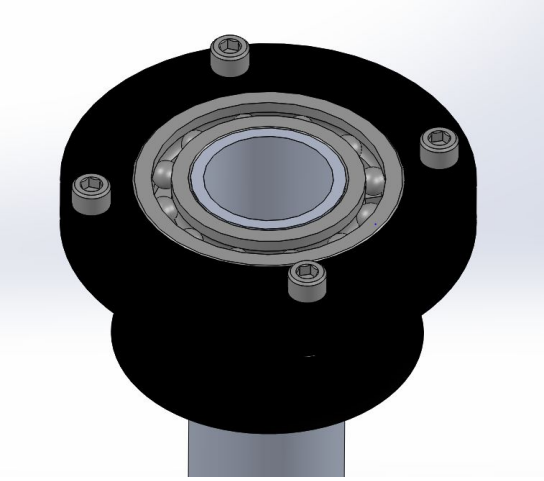

Figure 6: *Yaw System*

2.3 Electromechanical Design

2.3.1 RPM Monitoring

The team chose to use an E5 Optical Encoder from US Digital to measure the direct drive shaft rotational speed. The optical encoder is encased in a plastic casing that eliminates light interference that the prior team’s reflective sensor design encountered. Further, by using a 100 count per rotation encoder disk, a higher resolution of rotational speed accuracy can be achieved, when compared to the previous 4 count per revolution design. The optical encoder was mounted on the turbine drivetrain using a 3D printed mount. The output pulse-train timing from the encoder is measured with the turbine -side Arduino Uno and converted into an RPM measurement for control actions in the turbine.

2.3.2 Wind Speed Monitoring

In order to monitor the incoming wind speed from the wind tunnel, the team used a differential pressure sensor and a pitot tube that is mounted inside of the hollow driveshaft. Bearings were press-fit inside the shaft and the pitot tube placed inside the bearings. This allows the shaft to spin while the pitot tube remains stationary. Dynamic pressure is collected in front of the hub, while static pressure is measured inside the nacelle. The microcontroller uses the differential pressure measured to calculate incoming wind speed.

2.3.3 Braking

The team decided on the implementation of a smart braking system that would use a D625MW servo motor controlled by the turbine-side Arduino Uno. The servo motor will be attached to a disc

brake. The brake works by creating wind speed and RPM arrays that populate simultaneously from encoder and wind speed sensor measurements.. The most recent element in the wind speed array would be continuously checked until a reading of 11 m/s is achieved, at which point the corresponding RPM would be taken from the RPM array and set as the desired RPM. All RPM reading going forward will be based on the calculated RPM value based on the current wind speed. These calculated values would then be checked against the desired RPM and the servo motor would rotate from 0^{o} to 180^{o} depending on the degree of difference between the two RPM values in order to maintain the desired RPM at higher wind speeds. This approach was demonstrated to be successful in prior competitions. Unfortunately, testing availability was interrupted and a full calibration of the variable braking system with the new design elements of the turbine was not completed.

The emergency braking system utilizes two Actuonix PQ12 micro linear actuators, controlled by the turbine-side Arduino Uno, to clamp down on the spinning shaft of the turbine when the stop button is pressed, the turbine is disconnected from the PCC, or a wind speed greater than 21 m/s is detected. The bases of the linear actuators are placed in a 3D printed mold that is mounted inside the metal housing for the generator so that the rotating shaft for the turbine is resting in the divot of the mold. The end of the actuators are placed in another 3D printed piece that has a brake pad mounted above the shaft so that when clamped the shaft will be stopped. An important feature of the emergency brake is that once the linear actuators receive the signal to clamp down, they will remain clamped until another signal is received. This means that they will remain clamped even as the turbine loses power.

2.3.4 Current and Voltage Monitoring

The current monitoring system uses a 5A ACS712 current sensor and to provide proportional voltage readings that are then converted to current values through an Arduino.

A 10:1 voltage divider, composed of a 102kΩ resistor and a 11.3kΩ resistor, is placed at the PCC output connection to monitor the turbine output voltage. The reduced divider voltage output is used by the microcontroller to ensure that the turbine output voltage remains below the competition imposed 48 V maximum, Measured voltages greater than 46 V result in control system actions to reduce rotor speed, such as increasing power dissipation and/or adjusting disk brake application.

2.4 Electronic Design

2.4.1 Power Rectification

As the selected AFPMG produces a 3 phase AC voltage, a rectifier is required to produce the competition required DC output. An ideal diode rectifier was implemented on a custom printed board housed within the nacelle. The ideal diode rectifier uses 6 MOSFETS, whereas a Schottky diode rectifier would consist of 6 diodes. Although the gate logic associated with the MOSFETs may be more complicated, the diodes would result in a greater voltage drop, resulting in greater power losses. Using the simulated generator and rotor performance characteristics, theoretical power loss estimates were calculated. At a wind speed of 11m/s it is expected that the generator will produce approximately 1.2A. Given that a 1.2V drop can be expected across a pair of Schottky diodes, the power dissapated across these diodes approximately 4.8W. The selected MOSFETs for the ideal diode rectifier have an on resistance of 11.5mΩ. In the same scenario, the power loss in the MOSFETs is approximately 33.1mW. Although switching losses will result in slightly higher power dissipation, the ideal diode rectifier is expected to provide significant advantages to power generation capacity.

2.4.2 Power Conditioning and Management

Once the generated power is rectified it passes through electronics that are referred to as the power regulation and the control systems. Electrical schematics of the subsystems are provided in

Figures 10, 11, and 12 in the Appendix. The components of both subsystems reside on a custom circuit board in the nacelle.

The unregulated power from the ideal diode rectifier is connected in parallel with three electrical subsystems for power regulation, power dissipation, and output filtering. A constant, regulated voltage is required for the microcontroller, sensors, and actuators within the turbine. This voltage regulation is achieved using a wide-input LM2576 Buck converter, which converts the generated 14 V - 48 V into 9 V. Linear regulators are then used to convert this into the required 6 V actuator and 5 V sensor voltages.

The rectified power is also connected to a power resistor in series with a MOSFET connected to system ground. The gate of this MOSFET is controlled via pulse width modulation (PWM) from the turbine-side Arduino to increase the load on the generator. This power dissipation will occur to reduce the rotational speed of the rotor and reduce the output voltage to the PCC. The control system is programmed such that this power dissipation, possibly in combination with mechanical braking, will occur to prevent the PCC voltage from exceeding 46 V, ensuring that the output remains below the 48 V maximum.

Prior to connecting to the PCC, the rectified output is filtered with a 220 µH and 470 µF LC filter, creating a low-pass filter with a cutoff frequency of 494.95 Hz. This filtering will remove high frequency harmonics from the output resulting from the ideal diode rectifier switching and the 30 kHz switching frequency of the load-side maximum power point tracking (MPPT) system.

2.4.3 Maximum Power Point Tracking Load

For this wind turbine, power production must be maximized regardless of wind speed, a parameter that is exogenous to the turbine. The load consists of a 16 Ω power resistor and a low-side switch MOSFET. A 10:1 voltage divider and an ACS712 current sensor are used to monitor the voltage and current available to the load. A load-side Arduino Uno microcontroller implements a perturb and observe algorithm to control the effective resistance of the load by switching the MOSFET via PWM at a frequency of 30 kHz.

MPPT is performed on the load-side of the system to assist with cut-in power production and resetting of the servo motors during system restart. Refer to Figures 13 and 14 within the Appendix.

2.4.4 Circuit Design and Interconnections

As the 3-phase stator is made of 26 gauge copper wire, there are three 26 gauge wires that exit the generator. These three wires attach to the rectification pcb via a 3 position JST connector with 26 gauge wire. A 2 position (power and ground) JST connector with 26 gauge wire is used to connect the DC unregulated power from the rectification pcb into the power management pcb. Regulated power is then delivered to the sensors, actuators, a low current optocoupler and the turbine Arduino via similar JST connectors and 28 gauge wire. Regulated power also exits the power management pcb via a 2 position JST connector with 18 gauge two conductor Carol Brand cable and interfaces into the competition PCC with 15A PP15-45 Anderson Powerpole connectors. An additional 2 position JST connector exists to tie turbine electronics directly to the base plate, resulting in a near 0Ω resistance connection to ground. It is important to note that a single board is utilized for power management within the nacelle. This eliminates the need for external turbine control electronics.

The low current optocoupler is used for writing power measurements on the turbine side in real-time during testing. In the future, the optocoupler can be used to communicate voltage, current, wind speed, rotational velocity measurements and operational state parameters between the turbine and load Arduinos rather than having to measure these values for both. This development would eliminate the need for the voltage divider and current sensor within the Load subsystem. The

schematics in Appendix 3 include the components that allow for both methods of obtaining voltage and current values to the load-side Arduino. One method being direct measurement and the other would be to pass those measurements from the turbine-side Arduino to the load-side Arduino.

2.4.5 Energy Storage and Power Budget

The energy storage of the system is split between power management on the turbine side and the rectifier board inside the nacelle. In the turbine side there are eleven capacitors, ranging from 0.1uF to 680uF in capacitance, that provide a total energy storage of 9.4J.

The turbine has a D625MW servo motor and two PQ12 micro actuators that receive power from the 6V regulator. The servo motor has a current draw of 400mA while the two actuators have a combined current draw of 440mA, for a total current draw of 840mA for the mechanical systems. The power requirement of the mechanical actuators is 5.04W. Based on the projected maximum power production of 36.3W at 11 m/s, as seen in section 4.1.5, the servo and actuators are expected to be operational with approximately 31.26W sent to the PCC.

3 Control & Programming

3.1 Overview of Testing Tasks and Control States

The Finite-State Machine model was determined to be the best approach to control the various competition tasks. The system will take in inputs such as voltage, current, RPM, wind speed and enter a state based on the inputs. It was determined that all transitions between states had to be exclusive, meaning each state would have multiple transitions depending on the expected output.

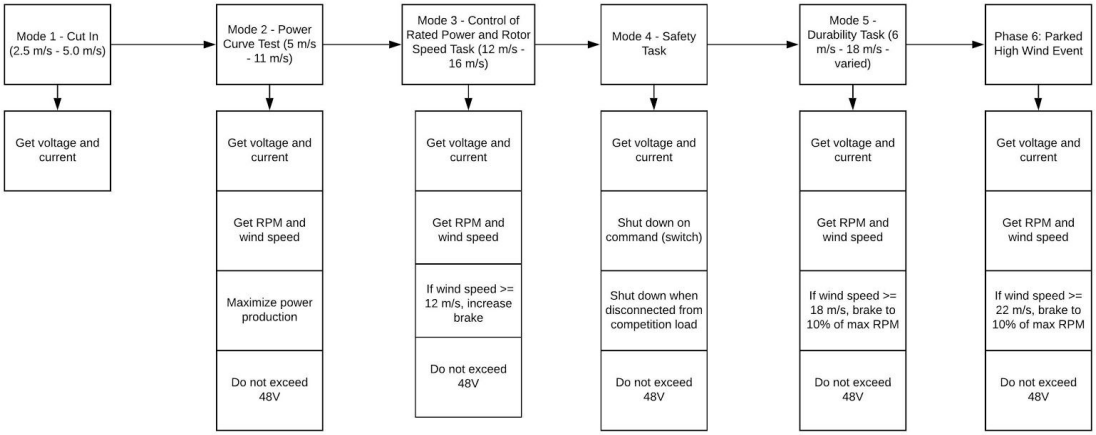

Figure 7: *Turbine Control State Diagram*

3.2 Programming and Initial Testing of Sensors and Actuators

To use the data collected from the sensors for braking, functions were created and called to populate arrays that would then have their most recent elements checked for values matching known wind speed requirements. Once it was found that the RPM given by the sensor and the calculated equation were equal, the desired RPM could then be compared to the expected RPM determined by the known wind speed and the difference between the two would then be used to determine the degree of braking needed to reach desired RPM. This would require more tests inside the wind tunnel to refine the calibrations.

4 Testing

4.1 Interim Deliverable Testing

A dynamometer was constructed and used to simulate rotary torque generated by the blades. This allowed for testing of sensors and electronics without putting the turbine in the wind tunnel. An optical encoder was mounted on the turbine drivetrain using a 3D printed mount and calculated the RPM output of the shaft using an Arduino Uno and the Arduino IDE displayed through the serial monitor on a computer. Using the dynamometer to simulate the rotary torque expected from the blades, the team was able to conduct initial tests on the power production of our generator iterations. It also allowed for testing of the RPM sensor in a controlled environment.

To test the strength of the turbine's rotors, they were spun at speeds of up to 4000 RPM using the dynamometer. The team was able to spin the rotors without failure at speeds of up to 2500 RPM, well above the expected maximum operating speed of ≅1100 RPM. Above 2500 RPM, the team experienced a failure in the hold of the set screws. To alleviate this issue, the hub was redesigned to have the same D-profile as the shaft, using geometry of the shaft as well as the set screws to ensure continued torque transfer.

4.2 Future Testing Plan

Had the team been able to continue testing after spring break, the dynamometer would've been used to test the responsiveness of the emergency brake and variable speed brake at various RPM inputs, as well as the team's custom made PCB boards. The team planned to have the full turbine assembled shortly after returning from spring break for wind tunnel testing. The team planned on using a purchased Magtrol TS 106 to ensure the rotary torque experienced in operation was in line with the expected torques at various operational points. Wind tunnel testing would also allow the team to test the yaw system and fine tune the turbine controls code.

5 Conclusion

This year, the JMU CWC prototype development team built upon previous competition experiences to enhance turbine performance and design aspects. By focusing efforts on increased *power production*, enhanced *control*, improved *safety*, and *ease-of-use*, the team developed an innovative and effective design in compliance with the Rules and Requirements for the competition. Intentional emphasis on blade and generator pairing using an iterative, modeling based approach, resulted in fixed pitch rotor and direct drive generator combination that was projected to maximize scoring in the power curve test. Accuracy of the control system was achieved by integrating a pitot tube within a hollow rotary drive shaft, thus allowing for direct measurement of the incoming wind speed. In this manner, wind speed can be used as the primary control parameter for turbine operation. To address the safety and parked high-wind event tasks, an additional clamping braking system was added to compliment the variable disk brake system. The newly added clamp brake's gearing system allows for the brake to remain engaged, even when power is reduced or lost, increasing the system safety and preventing runaway in extreme conditions. Finally, the team was able to increase the ease-of-use of the turbine by placing electronics within the nacelle. This simplifies the turbine setup and reduces the potential electrical connection failure points.

Due to the social distancing enforced in response to the onset of the COVID-19 pandemic, full construction and integration of the turbine systems was not possible. Although most subsystems had been fabricated and tested individually prior to spring break, complete turbine assembly and testing was slated to occur upon return to the JMU campus. Without access to supplies and laboratory capabilities, the team's focus shifted, allowing more time for subsystem analysis and review, along with a thorough system level review. The team was able to enhance the analysis done on various subsystems of the

turbine as a substitute for the testing that could not take place. Despite the inability to complete and test the prototype as planned, this additional analysis and design review provides additional confidence that the presented design meets the stated objectives and would perform well in the competition testing.

With the inability to complete the construction of the turbine and continue testing, the team was able to focus on the passing of information learned to the 2021 JMU CWC Team. Emphasis was placed on documenting all design decisions and supporting calculations online in a shared Google Drive folder. Weekly meetings were also held via WebEx to allow for the 2021 team to listen in and ask questions to facilitate the passing of knowledge. A Slack channel was also created to allow for quick communication between the teams. This transfer of knowledge and mentorship will position the JMU 2021 CWC team well to implement and improve upon aspects of the presented design to meet the next competition's objectives.

Finally, the team was able to gain knowledge and skills beyond the technical considerations associated with the prototype design. Through two wind energy development classes the team was exposed to the business development, siting, and finance considerations for wind energy development. Working closely with the project development team, the engineering team was able to make contributions associated with site selection and business considerations, extending our understanding of the engineering and business aspects of the wind energy industry.

JMU
CWC

The James Madison University Collegiate Wind Competition Turbine Design Team thanks you in advance for your time, your insights, and your commitment serving as competition judges. We thank you for your kind consideration and dedication to the field.

Appendices

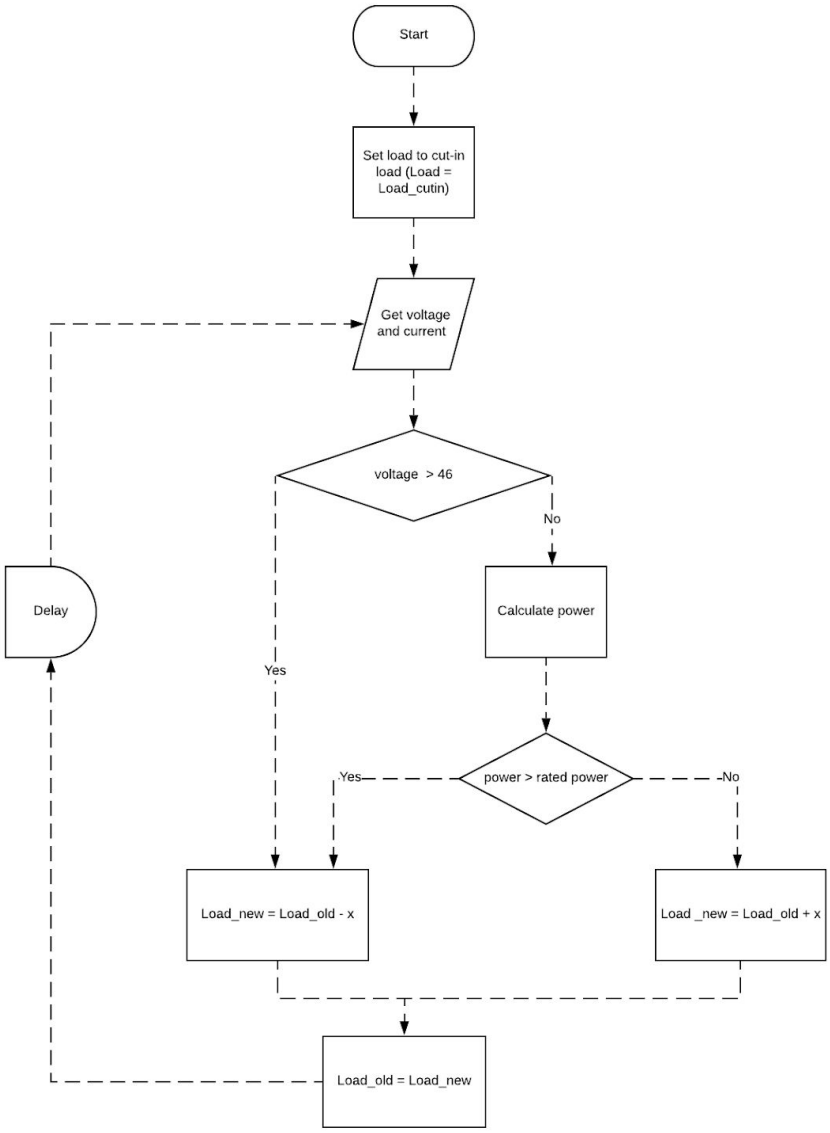

Figure 9: *MPPT Flow Model*

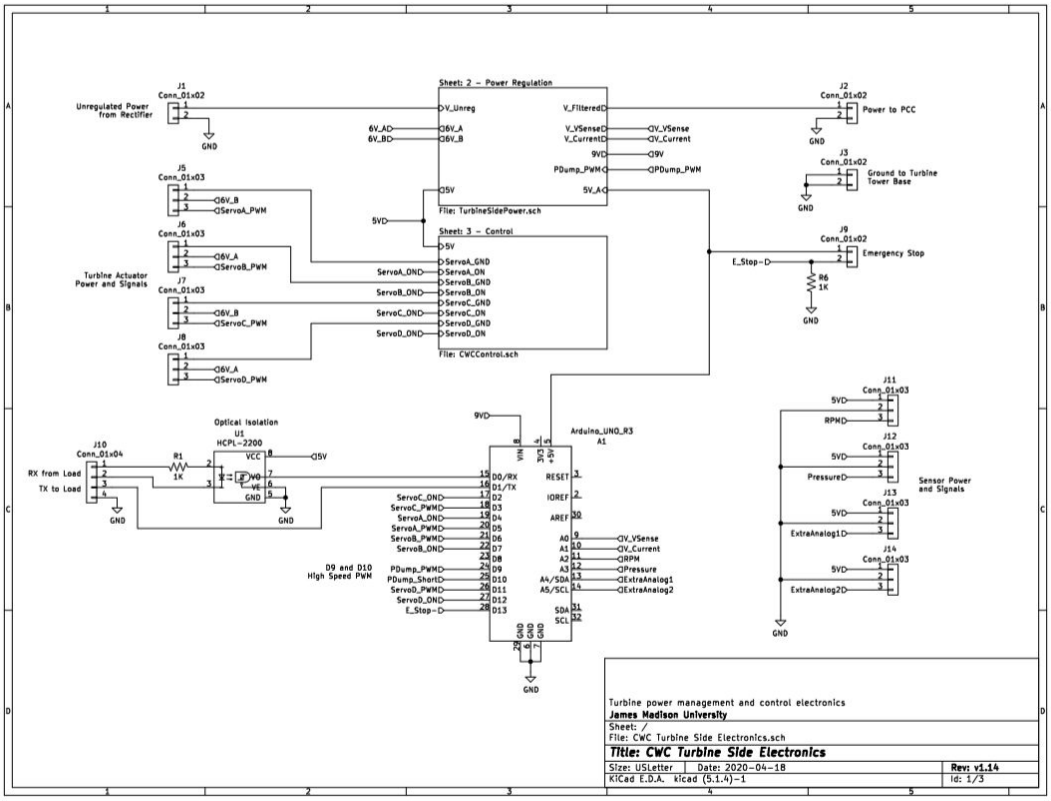

Figure 10: *CWC Turbine Side Electronics: Sheet 1*

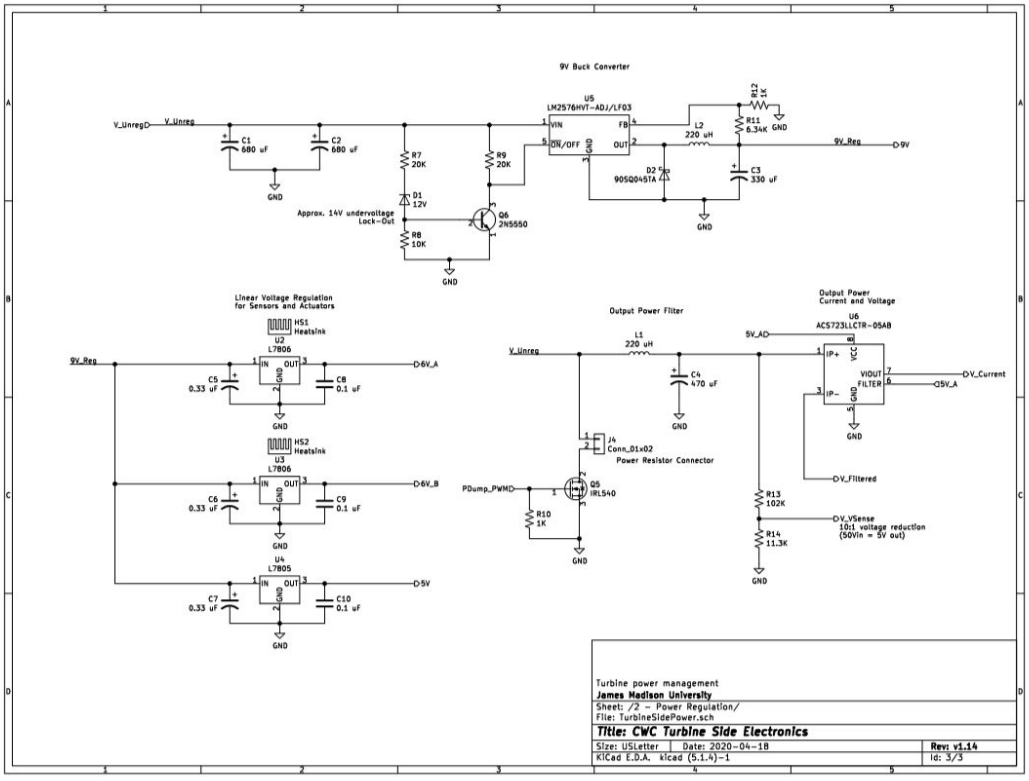

Figure 11: *CWC Turbine Side Electronics: Sheet 2*

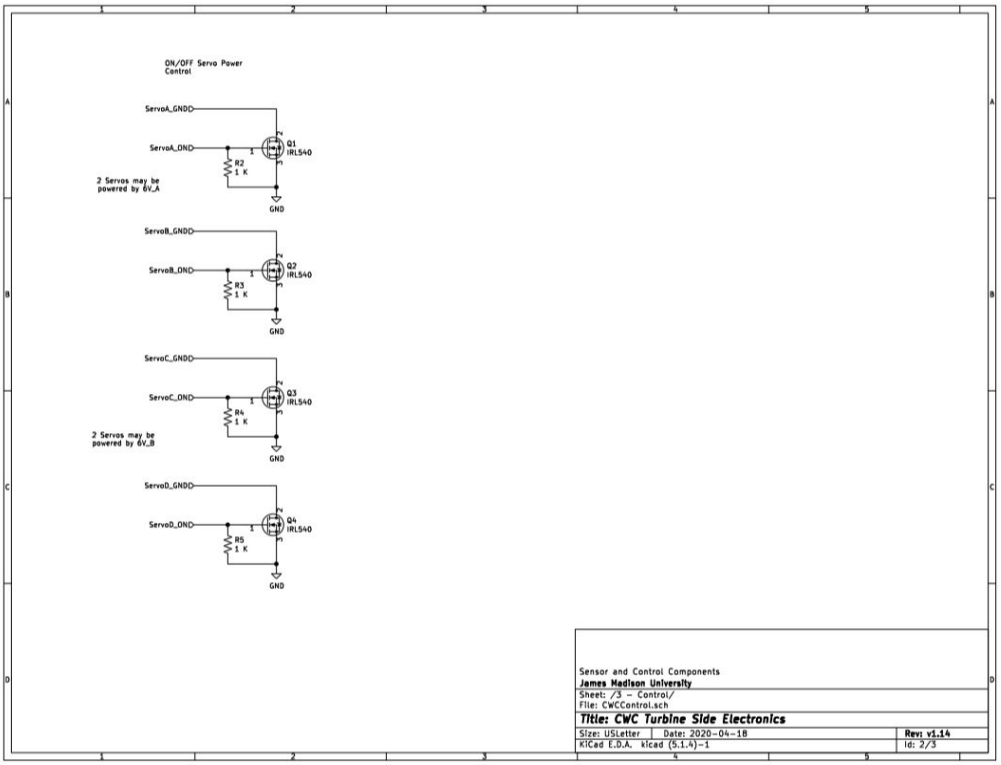

Figure 12: *CWC Turbine Side Electronics: Sheet 3*

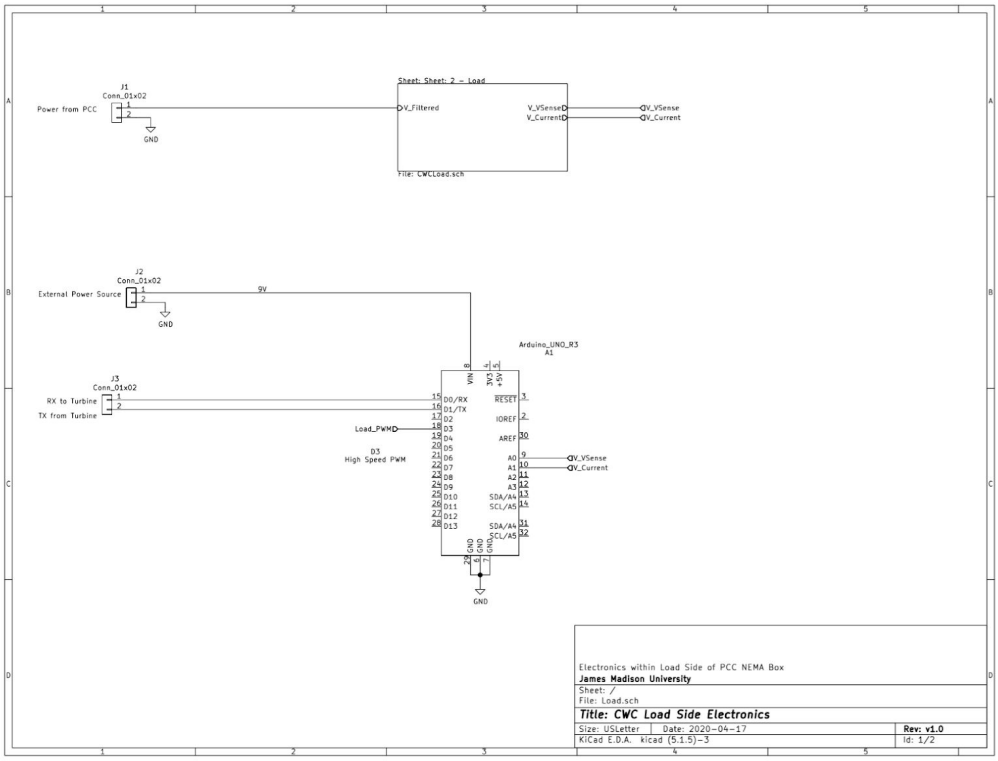

Figure 13: *CWC Load Side Electronics: Sheet 1*

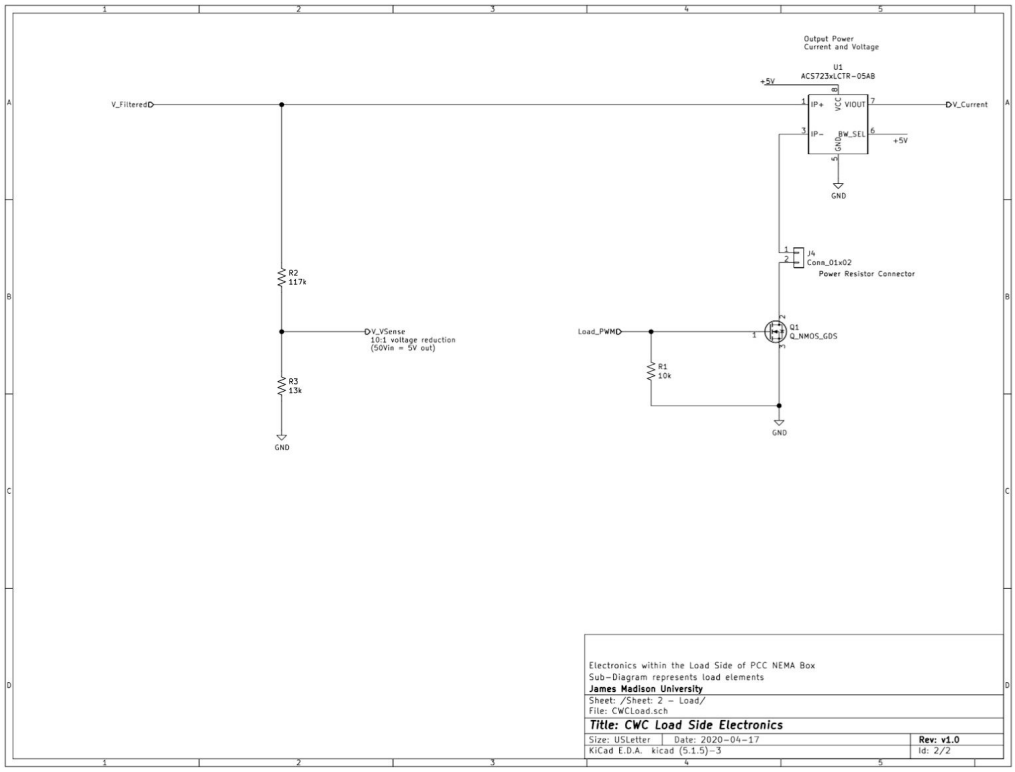

Figure 14: *CWC Load Side Electronics: Sheet 2*